






Cite this: *Green Chem.*, 2017, **19**, 3408

## The Hy-MASS concept: hydrothermal microwave assisted selective scissoring of cellulose for *in situ* production of (meso)porous nanocellulose fibrils and crystals†

Eduardo M. de Melo,  James H. Clark  and Avtar S. Matharu \*

The hydrothermal microwave-assisted selective scissoring (Hy-MASS) of depectinated orange peel residues (OPR), produced *via* conventional acid hydrolysis and acid-free microwave processing, to yield (meso)porous nanocellulose fibrils and crystals simultaneously in the absence of additional auxiliary reagents and/or mechanical treatment is reported. In the stepwise microwave hydrothermal treatment (MHT) of OPR from 120 °C–200 °C at 20 °C intervals, release of residual pectins and hemicelluloses is observed up to 180 °C producing nanocellulose fibrils (3–15 × 500–2000 nm). Beyond 180 °C, selective leaching/hydrolysis of amorphous regions occur to yield nanocellulose crystals (200–400 × 40–50 nm) and crystallites (5–15 × 40–50 nm). This selective, step-wise scissoring process is termed *Hy-MASS Concept*. Structure, morphology and properties of (meso)porous nanocellulose are strongly influenced by pectin extraction methodology employed. With acid depectinated OPR, deconstruction of the lignocellulosic matrix *via* microwave is hastened by approx. 20 °C with respect to acid-free microwave depectinated OPR.  $T_d$  of acid depectinated nanocelluloses (CMC) is ca. 350 °C compared to microwave depectinated nanocelluloses (MMC,  $T_d$ , varies 342–361 °C). Nanocellulose produced *via* microwave pre-treatment is (meso)porous: BJH pore size 5–35 nm; BET surface area, 1.5–107 m<sup>2</sup> g<sup>-1</sup>, and; BJH pore volume, 0.01–0.27 cm<sup>3</sup> g<sup>-1</sup>, when compared to acid pre-treated counterparts. The crystallinity index of CMC and MMC increases in two stages, 120–140 °C (ca. 8%) and at 180–200 °C (5–9%). XRD revealed presence of calcium salts, most likely calcium oxalate. The hydration capacities of nanocelluloses (12–23 g water per g sample) are much higher than their precursors or literature citrus nanocellulose.

Received 9th May 2017,  
Accepted 14th June 2017

DOI: 10.1039/c7gc01378g

rs.c.li/greenchem

## Introduction

Nanocellulose is a generic term given to cellulosic matter comprising one dimension in the nanometre range. Nanocellulose may be derived either from plant cell walls (top-down approach) or *via* bacterial fermentation of glucose (bottom-up approach).<sup>1</sup> Nanocellulose is synonymous with the terms nanocrystalline cellulose (NNC,  $D < 70$  nm and  $L < 500$  nm) or whiskers, nanocellulose (elementary) fibrils (NCF,  $D < 3.5$  nm and  $L < 1$  μm), microfibrillated cellulose (MFC,  $D < 100$  nm and  $L > 1$  μm), bacterial nanocellulose (BNC,  $D < 100$  nm and  $L > 1$  μm) and is a subject of intense interest due to its outstanding mechanical, optical, electronic and physicochemical properties.<sup>2–4</sup> In contrast to other cellulose fibres materials,

nanocellulose presents high surface area, aspect ratio and crystallinity which affects its surface chemistry and consequently high-value tunable, lighter and stronger bio-based materials can be produced from it.<sup>5–7</sup> Several works compares the mechanical properties of nanocellulose against other common reinforcement materials (such as steel and Kevlar) and in all cases nanocellulose presented outstanding performance.<sup>8–10</sup> Nanocellulose has been applied to a broad range of fields, ranging from biomaterials,<sup>9</sup> nanocomposites,<sup>11</sup> food additives<sup>12,13</sup> to electronics,<sup>14,15</sup> catalysis,<sup>16</sup> biomedical materials<sup>17</sup> and many more.<sup>18</sup>

Although nanocellulose applications has being studied since 1983, only recently its manufacturing became at least technically feasible.<sup>13</sup> To date, the production of nanocellulose at industrial scale has been restricted to just a few companies with a very limited production (totalling ca. 6000 kg per day).<sup>19</sup> In 2014, the global nanocellulose market was evaluated at \$250 million and forecast to grow by 19% by 2019.<sup>19</sup>

Conventionally, the industrial production of nanocellulose involves an acid catalysed (pre)treatment and/or enzymatic

Green Chemistry Centre of Excellence, Department of Chemistry, University of York, UK. E-mail: avtar.matharu@york.ac.uk

†Electronic supplementary information (ESI) available: Experimental data, ATR-IR, Py-GC-MS, CHN, HPLC sugar analysis and ICP-OES. See DOI: 10.1039/c7gc01378g



digestion of an appropriate cellulosic feedstock which removes polysaccharide–lignin complex holding fibrils together followed by dissolution of the amorphous regions *via* energy-intensive physical processing such as ultrasound and/or high mechanical shear the afford the desired nanocellulose fibrils (NCF) and/or nanocrystalline cellulose (NCC).<sup>4,20,21</sup> In contrast to conventional approaches, which are considered energy and time intensive, expensive and not green, many spin-offs and pilot-scale initiatives across North America, Europe and Japan have been exploring alternative methods for nanocellulose production,<sup>19,20</sup> resulting in an increasing number of patents over the last few years.<sup>13</sup> As an example of these advances, a recent patent claims to have produced nanocellulose from wood pulp at a low-energy input with aid of swelling agents (*e.g.* morpholine, potassium hydroxide) in addition to mechanical treatments.<sup>22</sup>

Herein, we report the *hydrothermal microwave assisted selective scissoring* (Hy-MASS) of depectinated orange peel residues to simultaneously produce (meso)porous nanocellulosic fibrils and nanocrystals in the absence any additional auxiliary reagent. This novel approach complements the current scenario of nanocellulose production by introducing environmental and economic advantages to the processing since the only inputs are biomass, water and energy (microwave) while the outputs (pectin, nanocellulose and sugar liquor) are all products of high-value, therefore virtually no waste is produced. García *et al.* (2016) have review production of nanocellulose derived from several food supply chain/agricultural residues, including citrus residue.<sup>2</sup> Mariño *et al.* (2015) reported the production of nanocellulose from orange peel waste by means of conventional treatments (physicochemical, enzymatic or a combination of both), but not commented on (meso)porosity.<sup>23</sup> Orange peel residues were chosen because of their under-utilisation within the context of a future orange waste or citrus peel biorefinery. The citrus industry produces approximately 70 million tons of crop per year,<sup>24</sup> of which 60–70% corresponds to oranges.<sup>25</sup> In the juice processing industry, at least 50% of the fruit is wasted, comprising peel, bagasse and seeds.<sup>26</sup>

Orange peel waste (OPW) is rich source of limonene, carotenoids, flavonoids, sugars, proteins and lignocellulosic matter (pectin, hemicellulose, cellulose and lignin), which alone corresponds to *ca.* 80% of OPW in dry weight.<sup>27</sup> Cellulose is the main biopolymer present in OPW, and an exploitable commodity, comprising around 40% of its dry weight.

Traditionally, pectin is extracted *via* acid hydrolysis of the peel and we have previously demonstrated microwave-assisted acid-free extraction of pectin.<sup>28–30</sup> Lignocellulosic biomass such as OPR can be activated by microwave treatment at relatively low temperatures (120–200 °C) and short residence time when compared to conventional chemical or enzymatic treatments.<sup>31</sup> Hydrothermal treatment of biomass under microwave irradiation generates ionic species (derived from free organic acids and water autohydrolysis)<sup>31,32</sup> that creates an *in situ* catalytic environment able to hydrolyse pectin, hemicellulose, lignin, amorphous cellulose and other components from the

cell wall matrix of biomass by different mechanisms such as proton transfer,<sup>33</sup>  $\beta$ -elimination,<sup>32,34</sup> ester/ether cleavage<sup>35</sup> and glycosidic bond cleavage.<sup>36,37</sup> Once these “hydrolysable” compounds are removed from OPR biomass, the remaining insoluble material should mainly comprise cellulose fibres. In this paper, we compare and contrast the effect of hydrothermal microwave processing of depectinated cellulosic residues arising from traditional (acid-assisted) and microwave-assisted (acid-free) on production and properties of nanocellulose. Changes in composition, structure and morphology of two types of mesoporous nanocellulose produced were studied by several techniques (NMR, XRD, ATR-IR, TGA, CHN, ICP-OES, porosimetry, SEM and TEM) and develop the Hy-Mass concept otherwise known as microwave assisted selective scissoring.

## Experimental session

### Materials

Orange peel waste (OPW) was obtained from sweet oranges (original from Spain) by processing the fruit in a juicer, where the collected peel was further chopped in to small pieces (around 10 × 10 mm) using a knife mill.

In this study, two methods for pectin extraction of OPW were undertaken to yield depectinated orange peel residues (OPR) from which mesoporous nanocellulose was produced, namely: i. conventional acid extraction (CAE) with 0.1 M aqueous-HCl (90–100 °C, 60 minutes under reflux), and; ii. additive-free microwave-assisted extraction method (MAE) developed in our centre<sup>28</sup> (Mars MW conditions: 4 g of OPW per 70 mL of water, 120 °C, 15 min, 1800 W). After work-up (filtration, washing residue with ethanol and drying at 50 °C for 48 h), depectinated dried OPR from both methodologies was subjected to hydrothermal microwave treatment (MHT) as outlined next. Distilled water was used throughout the experiments.

Lignin content<sup>38</sup> of OPR-CAE and OPR-MAE were found to be 0.50% and 1.50% respectively.

### Microwave hydrothermal treatment (MHT): general method

OPR samples were treated in a CEM Mars 6® closed vessel Microwave, operating to a maximum of 1800 W, 2.45 GHz using EasyPrep Plus® closed vessels (Teflon, 100 mL) to produce nanocellulose (see Fig. 1). Firstly, 1 g of dried OPR was mixed with 70 mL of distilled water giving a ratio of 1 : 70 (w/v) and applied to MHT at different temperatures ranging from 120–200 °C. Ramping time was fixed at 15 minutes, holding time of 10 minutes and high stirring was used. Afterwards, the resulting slurry was filtrated (while still hot), washed 3 times with ethanol (last wash with hot ethanol) and 2 times more with acetone (*ca.* 10× volume and 10–15 minutes each wash), vacuum-oven dried (40 °C, 48–72 hours, *ca.* 30–100 mbar) to afford the desired nanocelluloses. The latter were coded CMC when produced from conventional depectinated OPR whilst those from acid-free microwave assisted depectinated OPR were coded MMC. The three numbers fol-



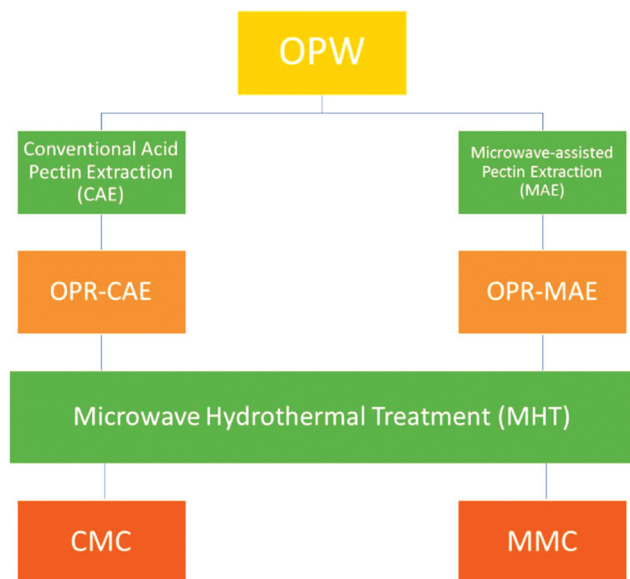


Fig. 1 Process diagram to produce nanocellulose from orange peel residue using MHT.

lowing their acronyms represent the MHT temperature in which they were treated (120 to 200 °C), for example; MMC120, refers to microwave depectinated OPR which has been subjected to microwave hydrothermal treatment at 120 °C, and; CMC-180, refers to conventional depectinated OPR that has been subjected to microwave hydrothermal treatment at 180 °C. Yield of nanocellulose was calculated as:

$$Y = (\text{mass of CMC or MMC} \div \text{mass of dried OPR}) \times 100.$$

### Instrumental analysis

For composition analysis and physicochemical characterization of CMC and MMC, Solid State  $^{13}\text{C}$  CP-MAS NMR, ATR-IR, powder XRD, TGA, CHN, SEM, TEM, nitrogen adsorption porosimetry, Py-GC-MS and ICP-OES analysis were performed. For image clarity samples for TEM were sonicated (ultrasound bath, 1500 W) for 30 minutes. Full instrument details are given in S1 (see ESI†). The water holding capacity test (WHC) was based on literature procedure<sup>39</sup> and is reported as water (g) per sample (g).

## Results and discussion

### Nanocellulose macroscopic features and yield

The CMC and MMC samples, as a result of MHT on both CAE and MAE orange peel residues, are depicted in Fig. 2 and their yields (with respect to dry OPR) are represented graphically in Fig. 3. As the temperature of microwave treatment (MHT) increases, an increasing brown colouration is observed probably due to products of the Maillard reaction, which are formed from the degradation/caramelization of sugars and their further reaction with residual proteins at high tempera-



Fig. 2 Nanocellulose samples produced by MHT of orange peel residue. Top row: MMC (120–200, left to right), and; bottom row: CMC (120–200, left to right).

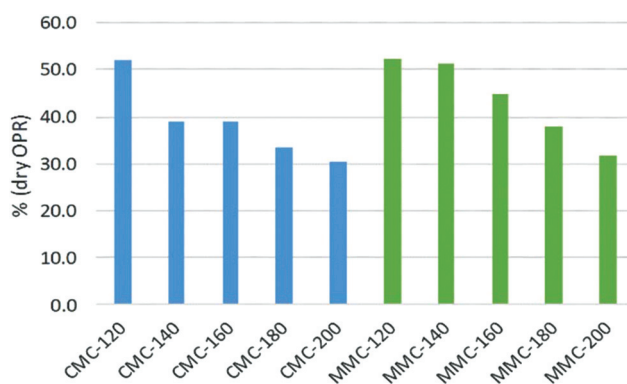


Fig. 3 Experimental yield (%) for produced nanocelluloses.

tures.<sup>40</sup> Similarly, Quitain *et al.*<sup>36</sup> showed that polysaccharides extracted from algae by hydrothermal microwave extraction have undergone browning at temperatures above 160 °C, which corresponds to similar browning observed in our samples.

As shown in Fig. 3 CMC and MMC yield decreases from 53% to 31% with respect to increasing MHT processing temperature, *i.e.*, from 120 °C to 200 °C, irrespective of initial OPR source. Mass loss is consistent with continual removal of pectinaceous matter at lower temperatures and depolymerisation (hydrolysis) of cellulosic matter and other structural polysaccharides to soluble oligosaccharides and monosaccharides units<sup>34,41,42</sup> at higher temperatures (at and above 180 °C). This is first indication of hydrothermal selective scissoring and the Hy-MASS concept.

Interestingly, the greatest mass loss is observed from CMC-120 to CMC-140 ( $\Delta$ , -13%) which then almost plateaus within the region 39–39% for the remaining temperatures. However, the corresponding hydrothermal treatment of OPR-MAE, *i.e.*, MMC-120 to MMC-140 shows negligible mass loss ( $\Delta$ , -1%) and thereafter an almost periodic, stepwise mass loss with increasing temperature. Such differences may be attributed to the harsher nature of CAE-OPR which removes



more pectinaceous matter and is more destructive to biomass (lignocellulosic matter) compared with the milder acid-free microwave treatment alone. HPLC sugar analysis of the aqueous liquors recovered after extraction of nanocellulose (see S2 in ESI†) complements this data, since rhamnose (a deoxy-sugar present in pectin polysaccharides) concentration in the liquor from CMC-140 ( $0.31 \text{ mg mL}^{-1}$ ) is 5 times higher than in MMC-140 liquor ( $0.06 \text{ mg mL}^{-1}$ ). This phenomenon exemplifies the onset of the Hydrothermal Microwave-assisted Selective Scissoring (Hy-MASS) concept.

### Nanocellulose ultrastructure

Cellulose nanofibrils (CNF) and cellulose nanocrystals (CNC) were successfully evidenced by TEM (Fig. 4). Inspection and measurement of the dimensions of CNF reveals microfibrils and elementary fibrils (varying from 3–50 nm in width and several  $\mu\text{m}$  in length) which are composed of dozens of indi-

vidual cellulose chains containing both amorphous and crystalline regions.<sup>43–45</sup>

From the MHT experiments at 200 °C cellulose nanocrystals (width 5–70 nm and length <500 nm) and nanocrystallites (width 3–10 nm and length 30–50 nm) were formed in MMC-200 and CMC-200, although nanocrystallites are only seen in CMC-200. These nanocrystals are derived from the crystalline regions of elementary fibrils after hydrolysis of embedded amorphous regions, which was proved to happen at temperatures above 180 °C.<sup>33,41</sup> The selective scissoring of amorphous regions produces nanocrystals reinforcing our Hy-MASS concept.

As we can see from Fig. 4, although CMC and MMC is mainly composed of cellulose nanofibrils and nanocrystals (at 200 °C), some residual amorphous matter entangled among them is also present. With increasing MHT processing temperature a gradual mobilization and hydrolysis of these dark grey amorphous clusters (composed of pectins, hemicellulose,

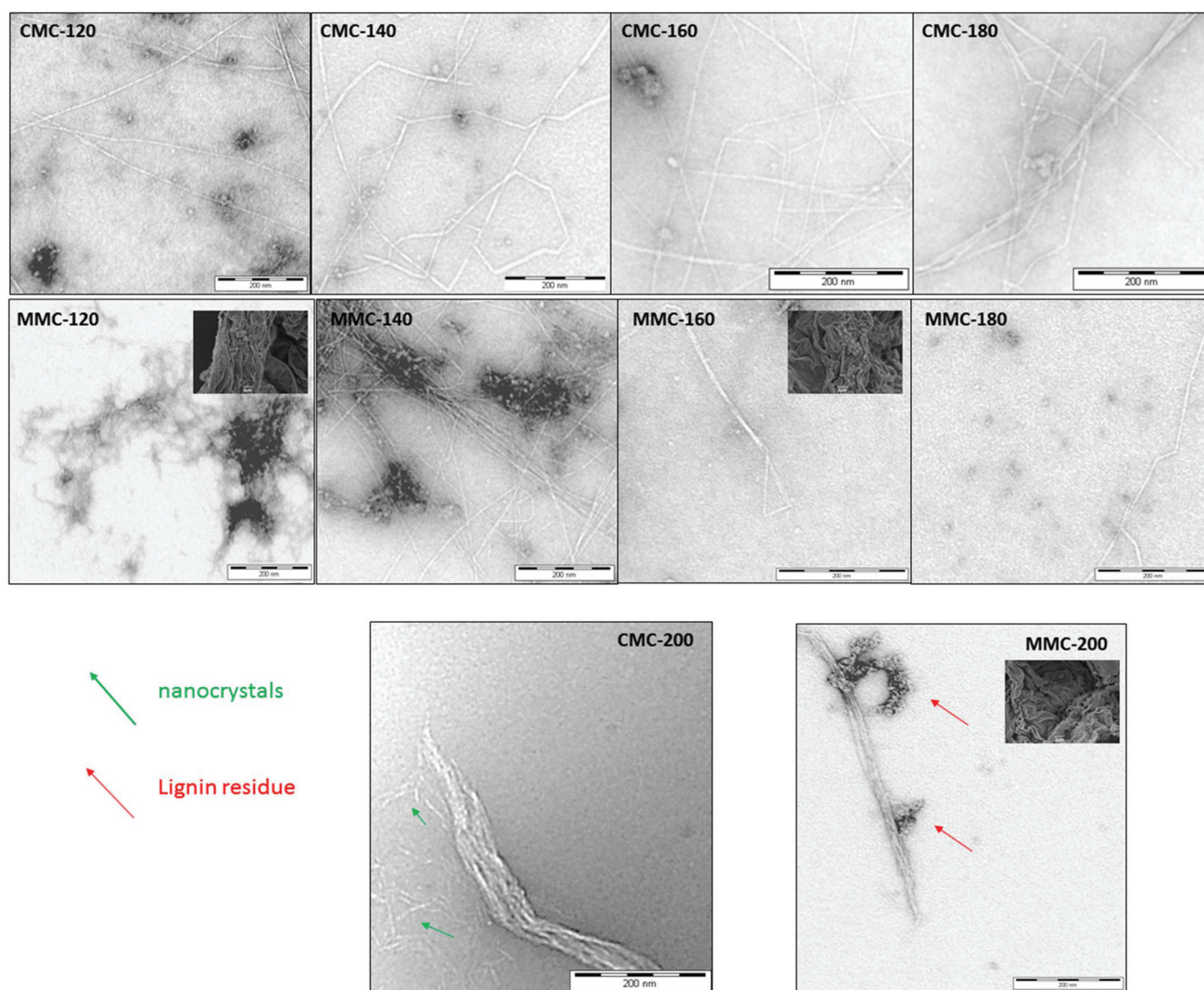


**Fig. 4** TEM images of CMC and MMC samples (scale bar = 200 nm). Arrows indicate the presence of nanocrystallites of cellulose (green) and possible residual lignin fragments (red). SEM images are shown as insets for MMC-120, MMC-160 and MMC-200 samples (scale bar = 2  $\mu\text{m}$ ).



lignin and possibly amorphous superficial cellulose) is achieved. However, even at 200 °C, some of these recalcitrant clusters (which are believed to be mainly composed of residual lignin fragments)<sup>45,46</sup> can still be found at the surface of nanofibrils and crystals. In a similar manner, gradual morphological changes are also observed on selected samples of MMC type (120, 160 and 200) by SEM at lower magnification, as shown in the insets of Fig. 4. These changes further confirm the deconstruction of the cellulosic structure of the biomass by Hy-MASS.

These observations translate the concept of Hy-MASS happening in at least two main stages: i., the gradual scissoring of the “coating” and entangled amorphous content from the nanocellulose fibrils surface from 120–180 °C and ii., the scissoring of the amorphous regions of cellulose embedded in the elementary fibrils happening between 180–200 °C and yielding cellulose nanocrystals in addition to nanofibrils.

Anticipating the following discussion on nanocellulose composition and properties, all spectroscopic analyses performed are in good agreement with the abovementioned data and concepts. In particular, degree of crystallinity calculated from XRD data presented a pattern in which the two Hy-MASS stages can be clearly observed (section *Crystallinity Index*).

### Nanocellulose chemical composition and characterisation

**Solid state <sup>13</sup>C CP-MAS NMR analysis.** The <sup>13</sup>C CP-MAS NMR spectra MMC and CMC samples are stacked and grouped accordingly as shown in Fig. 5. Each individual spectrum shows characteristic signals for cellulose carbon (C1 to C6).<sup>47,48</sup> Both CMC-120 and MMC-120 show strong evidence of a carbonyl carbon at *ca.* 172 ppm which may attributed to

residual pectinaceous matter and/or strongly bound cell wall polysaccharides (*e.g.* hemicelluloses) in the initial OPR.<sup>49</sup> Weak signals are detected at 25–40 ppm associated with rhamnose, fucose or acetyl methyl residues within pectin structure.<sup>48,50,51</sup> On increasing MHT processing temperature these signals disappear, *i.e.*, no longer evident after 160 °C, suggesting hydrolysis and depolymerisation of such matter from the cell wall matrix<sup>29,36</sup> and correlate with HPLC sugar analysis of the hydrolysate mentioned earlier. Moreover, a change in the ratio of cellulosic surface/amorphous C4 and C6 (84 ppm and 62 ppm respectively): interior/crystalline C4 and C6 (89 ppm and 65 ppm respectively)<sup>45,52</sup> is observed (black arrows in Fig. 5), suggesting that amorphous contributions from cellulose microfibrils surface is also gradually hydrolysed during the treatment. The cellulosic character of the materials increases, which correlates well with thermogravimetric data as discussed next.

**Thermogravimetric analysis (TGA).** TGA thermograms (Fig. 6) are consistent with those of cellulose<sup>53</sup> and show evidence of residual non-cellulosic matter for low temperature MHT samples, *i.e.*, 120 °C and 140 °C. The DTG thermograms for CMC and MMC samples (Fig. 6) show three mass loss bands, namely, i. loss of moisture and volatiles (around 4–5%;  $T_d = 80–100$  °C); ii.  $T_d$  *ca.* 250 °C due to the decomposition of residual pectins and hemicellulose which becomes less evident in samples treated from 160–200 °C, and; iii.  $T_d$  *ca.* 340–360 °C, this is associated with largest mass loss due to cellulose decomposition.<sup>54–56</sup>

Interestingly, cellulose  $T_d$  for all CMC samples remains fairly constant or appears to be MHT processing temperature independent. Again, this may be associated with the harsher

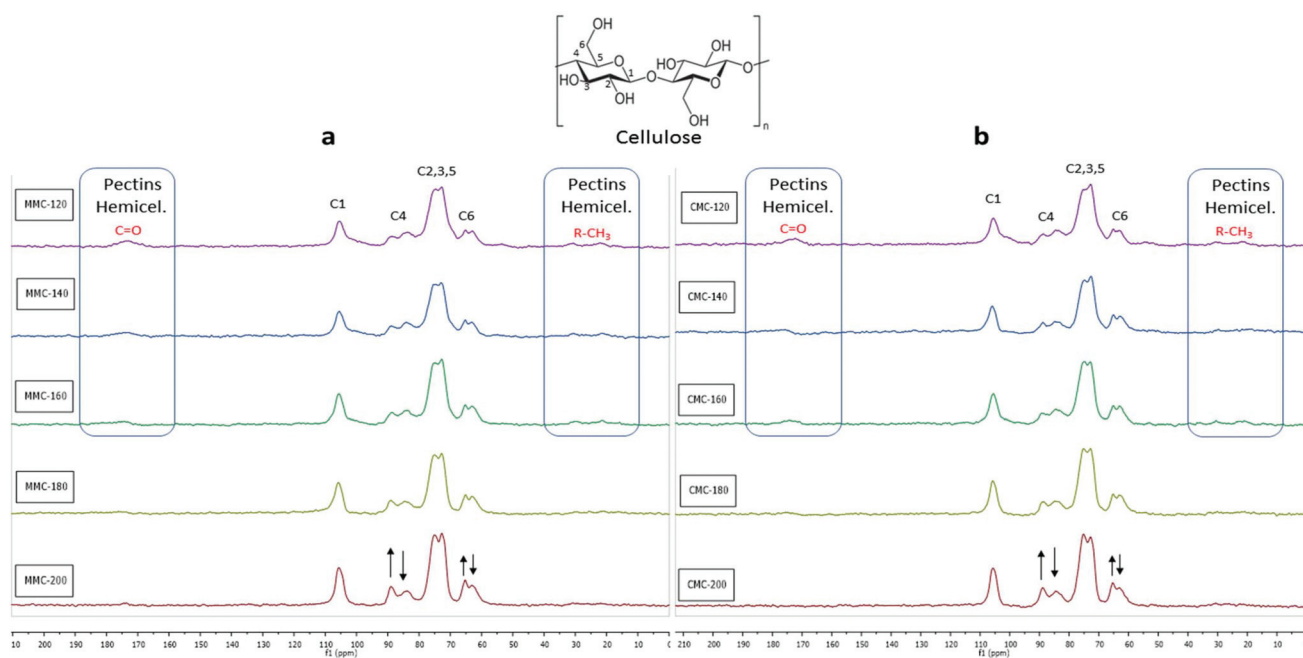


Fig. 5 <sup>13</sup>C CP-MAS NMR spectra of MMC (a) and CMC (b) samples with a labelled illustration of cellulose molecule. Assignments for pectins/hemicellulose groups are highlighted in red label. Arrows show the ratio of crystalline/interior : amorphous/surface cellulose.



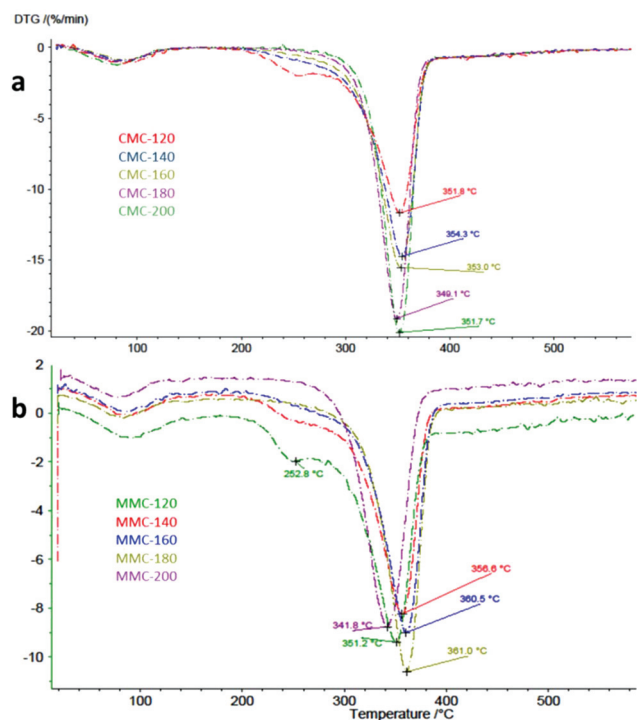


Fig. 6 DTG thermograms of CMC (a) and MMC (b) samples.

initial acid treatment employed with respect to CAE-OPR which seems to remove a greater proportion of cellulosic bound matter and hence fixes cellulosic structure (Fig. 6a). The same does not happen for MMC samples (Fig. 6b), in which cellulose  $T_d$  shifts significantly: MMC-120 ( $T_d$ , 351.2 °C); MMC-140 ( $T_d$ , 356.6 °C); MMC-160 ( $T_d$ , 360.5 °C); MMC-180 ( $T_d$ , 361.0 °C), and; MMC-200 ( $T_d$ , 341.8 °C), implying that the initial removal of pectin *via* MAE has a less destructive effect on cellulosic matter and related constituents. In fact, the latter (MMC-200) was expected to have the highest cellulose thermal stability compared with respect to its lower temperature homologues (due to its highly crystalline cellulose content as discussed next) but actually gave the lowest  $T_d$  (341.8 °C) which decreased by 20 °C compared with MMC-180. Replicates of MMC-200 were run, however same thermogram pattern was achieved. This shift could be related to the higher content of calcium present in that sample as discussed in the following section.

**X-ray powder diffraction analysis (XRD) and elemental analysis – the curious case of calcium.** The XRD traces of MMC and CMC samples at different processing temperatures depicted in Fig. 7. Apart from the characteristic crystalline cellulose XRD pattern observed (Fig. 7,  $2\theta$  peaks at *ca.* 16.5°/22.5° and 34.5°), additional peaks at *ca.* 15°/24° and 30° were identified in MMC samples only. These are postulated as calcium salts, most likely  $\text{CaC}_2\text{O}_4$ , which is known to be synthesized by plants and stored in their tissues (cell wall and vacuoles) and has been evidenced in the literature.<sup>57,58–60</sup> Comparing diffraction patterns of all the MMC samples, *i.e.*, MMC-120 to MMC-200, shows that  $\text{CaC}_2\text{O}_4$  peaks become more discernible

and intense, especially at 200 °C. This also correlates with the fact as more organic content is solubilised, depolymerised and hence extracted at MHT processing temperatures which heightens the presence of any insoluble salts embedded in the cellulose fibrils such as  $\text{CaC}_2\text{O}_4$ . To further confirm the presence of  $\text{CaC}_2\text{O}_4$  and other minerals in MMC samples, MMC-200 was washed with 2 M aqueous HCl using the protocol described by Perez-Pimienta *et al.*<sup>59</sup> As expected, the “extra” peaks disappeared (Fig. 8), inferring the leaching of acid-soluble mineral salts from cellulosic matter. Mineral salts by XRD were not detected in CMC samples but this is not to say they are not present as revealed by ICP-OES (S3 in ESI†). An elemental analysis of the nanocellulose samples and their respective precursor (OPR-CAE and OPR-MAE) was performed by ICP-OES. S3 shows the distribution of the 5 most abundant identified species. Interestingly, calcium was the most abundant inorganic species (3000 to 10 000 ppm) which corroborates calcium salts detected by XRD in MMC samples. In fact, the CMC samples contain calcium but at least 50% less than their MMC counterparts, again supporting the role of acid treatment in effectively leaching mineral salts (as well as pectates) at the depectination step. Interestingly, copper was detected which may be due to the presence of copper-mediated metallo-enzymes such as oxidases known within citrus peel.<sup>61</sup>

CHN analysis (S4 in ESI†) of nanocellulose samples gave 0.81% N content which equates to an average protein content (calculated from the N content using a conversion factor of 4.64)<sup>62</sup> of 3.8%. Assuming that N content is solely due to proteinaceous matter, this implies that residual enzymes and other proteins<sup>31</sup> might be present in the nanocellulose samples.

The acid-free MAE method to depectinate OPW appears to retain a higher concentration of inorganic salts in the resultant OPR than compared with CAE, which effectively leaches acid-soluble salts. The presence of calcium salts in cellulosic matter may be beneficial for certain applications where calcium is added, for example in food sector<sup>46</sup> catalytic nanoparticles,<sup>17</sup> displays<sup>44</sup> or composite materials.<sup>63,64</sup> The applications of such materials are on-going. The acid-free MAE method also appears to retain a significant nitrogen content which in combination with mineral salts could seek applications as a bio-fertiliser.

**Infrared analysis (ATR-IR).** In agreement with the already discussed results, ATR-IR analysis supports the presence of cellulose as the main component of the produced biomaterial, as well as pectin/hemicellulose/lignin.  $\text{CaC}_2\text{O}_4$  salts may be tentatively identified but are masked by stronger cellulosic matter skeletal vibrations. Assignments of characteristic absorption bands for these compounds<sup>55,59,65</sup> are summarized in Table 1 (S5-I in ESI†) and spectra (S5-II in ESI†). Absorption bands attributed to the carbonyl group (*ca.* 1730  $\text{cm}^{-1}$ ) from residual pectins, hemicellulose and lignin structures present in CMC and MMC decrease in intensity as MHT processing temperature increases, which confirms its gradual removal from OPR during the microwave treatment. On the other hand,  $\text{CaC}_2\text{O}_4$  recalcitrance may be tentatively confirmed by the pres-



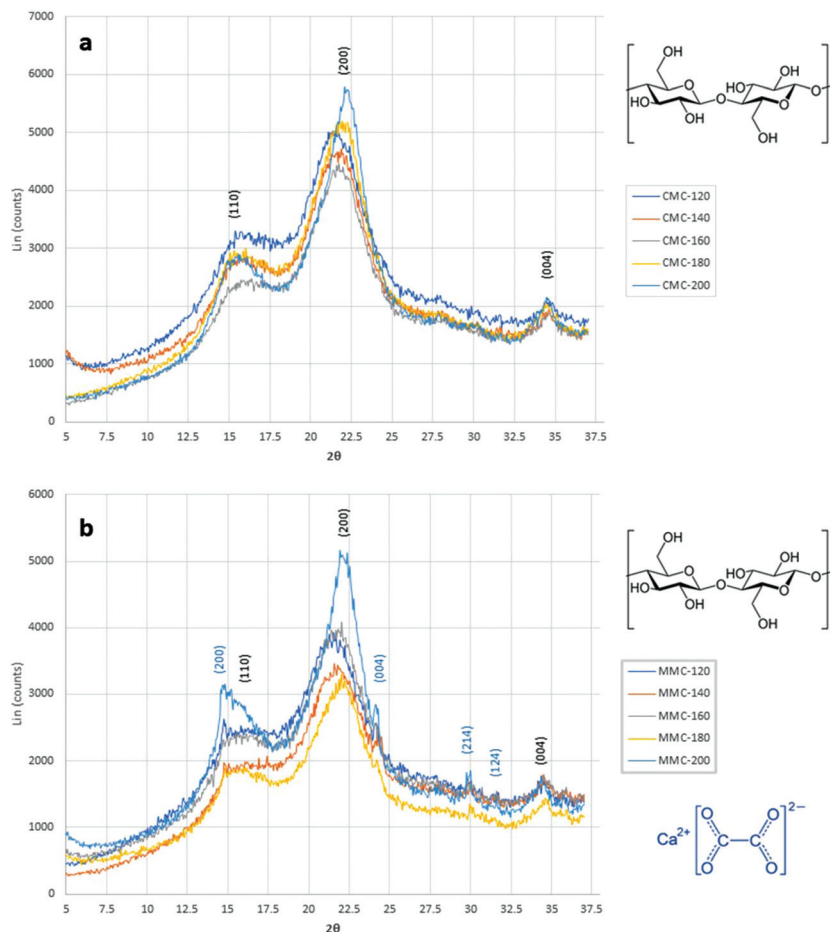


Fig. 7 XRD diffractograms of CMC (a) and MMC (b) samples with cellulose peaks assigned in black and CaC<sub>2</sub>O<sub>4</sub> peaks in blue. Planes were coded according to Miller index (*hkl*).

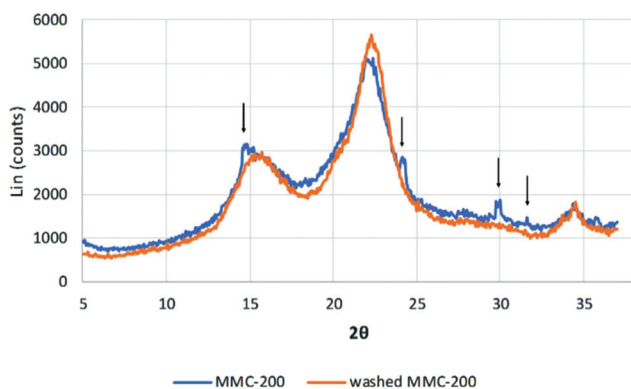


Fig. 8 XRD diffractograms of MMC-200 and acid washed MMC-200. Arrows emphasizes the removal of calcium oxalate peaks upon acid wash.

ence of its characteristic absorption bands at *ca.* 1620–1630 and *ca.* 1320 cm<sup>-1</sup>.<sup>59</sup> Evidence for the presence of lignin in the samples can be confirmed by the absorptions of the aromatic ring stretching around 1516 cm<sup>-1</sup> and 1240 cm<sup>-1</sup>,<sup>65</sup> but due to its low content in dried orange peel residue (*ca.* 1–2%) absorp-

tions related to its structure is quite weak in intensity when compared to the polysaccharides ones. Likewise, Pyrolysis GC-MS (S6 in ESI<sup>†</sup>) further confirmed lignin presence by its pyrolysis products,<sup>66,67</sup> such as: phenolics, benzenetriol, vinyl-guaiacol, among other aromatics.

### Nanocellulose morphology and physical properties

**Porous structure analysis.** During the work-up of nanocellulose, the solvent exchange step with ethanol and acetone is crucial to preserve its porous structure. The porosimetry data for CMC and MMC samples is shown in Fig. 9. According to this data, most of the produced nanocellulose presented improved porous structure when compared against their precursors (depectinated OPR-CAE and OPR-MAE presented negligible porosity; surface area and pore volume close to zero). In Fig. 9a a steady increase of BET specific surface area and BJH pore volume for MMC samples is seen up to 180 °C which agrees with the gradual removal of non-cellulosic matter, however at 200 °C (MMC-200) surface area and pore volume values have a significant decrease, which could be related to blockage of open pores by residual lignin as previously reported for other biomass.<sup>45,68,69</sup> Surprisingly, CMC samples (Fig. 9b)



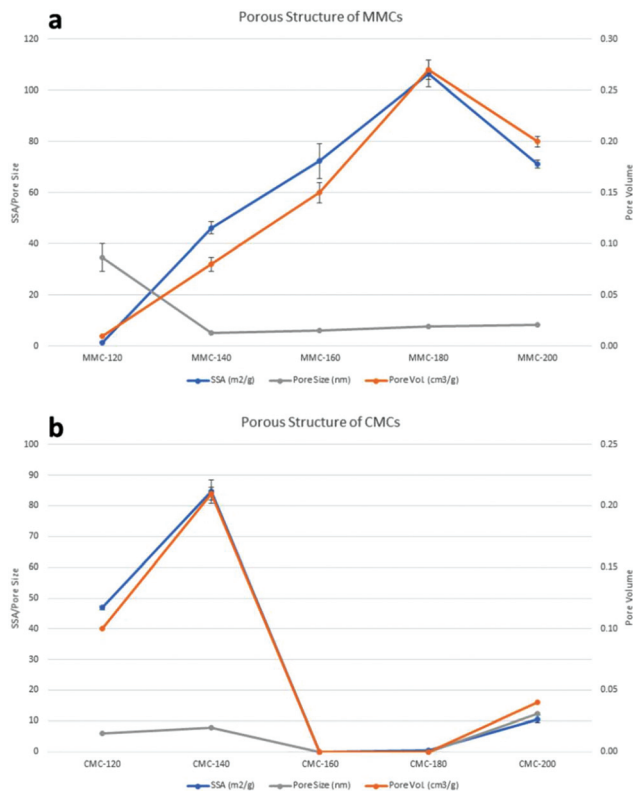


**Fig. 9** Porosimetry data (BET Specific surface area – SSA, BJH pore volume and BJH average pore size) for MMC (a) and CMC (b) samples. Units for each parameter is described in the legend. Error bars represents standard deviation ( $n = 3$ ).

presents a different pattern compared to MMC. Considerable porosity is only found up to 140 °C and again at 200 °C which implies that in that temperature interval some interesting structural changes has happened (e.g. pore collapse or blockage).

Regarding BJH pore size of cellulose samples (Fig. 9), they all lie in the range of 2–50 nm. Thus, according to the IUPAC pore size classification, nanocellulose produced from orange peel waste can be defined as mesoporous biomaterial. Previous works from our research group have used similar microwave treatment to produce mesoporous cellulose from depectinated citrus peel<sup>29</sup> and mango peel<sup>30</sup> with similar porosity to the nanocellulose produced in this work, showing that MHT is a flexible feedstock “insensitive” technology to produce high-value chemicals and materials from a broad range of biomass without the need of chemical additives.

**Crystallinity index.** According to Fig. 10, a significant increase in the crystallinity index (CrI) for both types of nanocellulose is seen in relation to their precursors (approx.  $\Delta = 3$ –21% for CMC and 0–13% for MMC) as well as with the increase of MHT temperature ( $\Delta = 19\%$  for CMC and 14% for MMC). As previously discussed in section *Nanocellulose Ultrastructure*, this effect can be directly linked to two major stages of the Hy-MASS concept. First, the CrI increase in nanocellulose from 120 °C to 180 °C is associated with gradual, selective removal (scissoring) of the amorphous pectins, hemi-

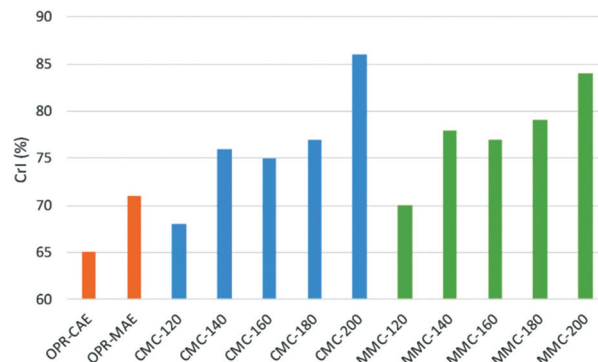


**Fig. 10** Crystallinity Index (CrI) calculated from XRD data for CMC, MMC and their respective precursors (OPR-CAE and OPR-MAE).

celluloses and lignin from the cellulosic matrix by cleaving susceptible chemical bonds,<sup>31,35</sup> which agrees with previously discussed data (NMR, IR, XRD and TGA.). Secondly, during microwave treatment of lignocellulosic biomass, softened amorphous regions embedded in the cellulose microfibrils interacts with microwave energy by dipolar polarization which generates a proton transfer mechanism at temperatures above 180 °C,<sup>33,41</sup> hydrolysing those regions by “selective scissoring” causing a significant CrI increase in samples treated at 200 °C.

**Water holding capacity.** The hydration capacity or water holding capacity (WHC) of nanocellulose samples is shown in Fig. 11. All samples presented higher (approximately 1.5 times higher) or comparable hydration capacity in comparison with their precursors (OPR-CAE and OPR-MAE) and comparable literature data.<sup>39</sup> Larger particle size and negligible surface area could be the factors behind the lower WHC of the precursors against nanocelluloses. Among nanocellulose types, there was no significant difference between CMC and MMC. For both types, the ones that were produced at 200 °C presented the lowest values (12 g water per g for CMC-200 and 16 g water per g for MMC-200) while the average value for the other samples

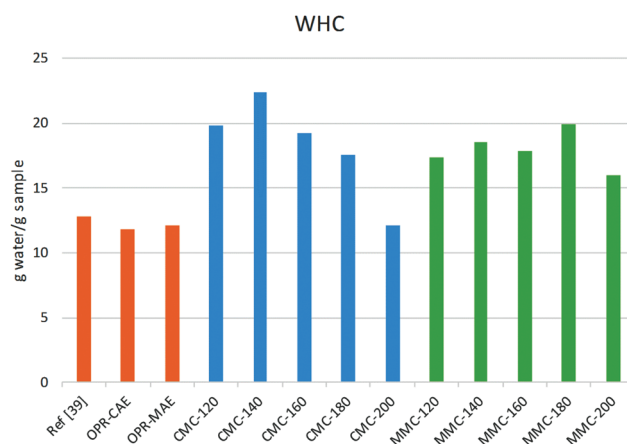


**Fig. 11** WHC values (g of water per g of dry sample) of nanocellulose from ref. 39, precursors (OPR-CAE and OPR-MAE) and produced nanocelluloses (CMC and MMC). Values are expressed as average of duplicate experiments.





ranged around 20 g water per g of sample. This could be related to the higher content of nanocellulose crystals against fibrils in those samples, as confirmed by TEM and XRD data (CMC-200 and MMC-200 presents higher CrI). Since nanocellulose crystals and crystallites are derived from crystalline regions of elementary fibrils where cellulose chains are strongly bound by intra/inter hydrogen bonds, it is expected that the hydration capacity of these crystals will be much lower than the fibrils, which are able to better retain water due to the presence of amorphous regions which contains hydroxyl groups available for hydrogen bonding with water.<sup>40,70</sup> Moreover, insoluble cellulose fibres are known to hold water by entangling water in their fibril network and by swelling properties.<sup>70</sup>

## Conclusions

The novel methodology used in this work (additive-free microwave hydrothermal treatment) has been demonstrated to be a suitable green alternative for the production of highly crystalline and mesoporous nanocellulose from orange peel residue *via* a process of selective scissoring otherwise known as the Hy-MASS concept.

The mesoporous nanocellulose produced has been thoroughly characterized, where presence of trace elements (calcium, copper) and molecules (salts, pectin, hemicellulose and lignin) were confirmed by several spectroscopic techniques. A direct relationship of microwave treatment temperature and “purity” of nanocellulose samples were also identified through those techniques plus thermal analysis, where higher process temperatures lead to more purified and more crystalline nanocellulose fibrils, although lignin traces seem to be recalcitrant even at 200 °C. Traces of calcium salts were recalcitrant in MMC samples and could only be removed by acid wash. The nano- and porous-structure of nanocelluloses was successfully confirmed by TEM and porosimetry analysis, respectively. Due to the fact that microwave treatment allows more control over the experiment parameters (specially temperature), samples treated only under microwave throughout the process (MMC) presented a more regular pattern for crystallinity index and porosity (specific surface area, pore volume, pore size), which was not observed for CMC samples (depectinated with acid treatment). Thus, reproducible results are better achieved when using MHT for both, pectin extraction and nanocellulose production. The hydration capacity of nanocellulose samples were found to be higher than their precursor or from literature data, which is very promising in food applications.

## Acknowledgements

The Authors would like thank CNPq, Conselho Nacional de Desenvolvimento Científico e Tecnológico (Brazil), for scholarly funding of Eduardo Melo to undertake research at University of York, UK, Dr Meg Stark for TEM analysis and Dr Hannah Briers for HPLC sugar analysis.

## References

- D. Klemm, F. Kramer, S. Moritz, T. Lindström, M. Ankerfors, D. Gray and A. Dorris, *Angew. Chem., Int. Ed.*, 2011, **50**, 5438–5466.
- A. García, A. Gandini, J. Labidi, N. Belgacem and J. Bras, *Ind. Crops Prod.*, 2016, **93**, 26–38.
- A. Dufresne, *Mater. Today*, 2013, **16**, 220–227.
- I. Oke, *Stud. Undergrad. Res. Guelph*, 2010, **3**, 77–80.
- K. J. De France, T. Hoare and E. D. Cranston, *Chem. Mater.*, 2017, **29**, 4609–4631.
- A. Ferrer, L. Pal and M. Hubbe, *Ind. Crops Prod.*, 2017, **95**, 574–582.
- C. S. Davis, R. J. Moon, S. Ireland, L. Johnston, J. A. Shatkin, K. Nelson, E. J. Foster, A. M. Forster, M. T. Postek, A. Vladar and J. W. Gilman, in *2014 TAPPI International Conference on Nanotechnology for Renewable Materials Report*, National Institute of Standards and Technology, Gaithersburg, MD, 2015, pp. 1–42.
- R. J. Moon, A. Martini, J. Nairn, J. Simonsen and J. Youngblood, *Chem. Soc. Rev.*, 2011, **40**, 3941.
- H. M. C. Azeredo, M. F. Rosa and L. H. C. Mattoso, *Ind. Crops Prod.*, 2017, **97**, 664–671.
- A. Dufresne, in *Nanocellulose: From Nature to High Performance Tailored Materials*, Walter de Gruyter, 2012, pp. 1–42.
- R. Johnson, A. Rosso and N. Semansky, *Fabrication and Testing of Arabinan Cellulose Nanocomposites*, California Polytechnic State University, 2014.
- G. Ström, C. Öhgren and M. Ankerfors, *Nanocellulose as an additive in foodstuff*, 2013.
- C. Gómez H., A. Serpa, J. Velásquez-Cock, P. Gañán, C. Castro, L. Vélez and R. Zuluaga, *Food Hydrocolloids*, 2016, **57**, 178–186.
- M. Park, D. Lee, S. Shin, H.-J. Kim and J. Hyun, *Carbohydr. Polym.*, 2016, **140**, 43–50.
- A. Carlsson, *Structural and Electrochemical Properties of Functionalized Nanocellulose Materials and Their Biocompatibility*, Acta Universitatis Upsaliensis, 2014.
- P. Huang, Y. Zhao, S. Kuga, M. Wu and Y. Huang, *Nanoscale*, 2016, **8**, 3753–3759.
- C. Salas, T. Nypelö, C. Rodriguez-Abreu, C. Carrillo and O. J. Rojas, *Curr. Opin. Colloid Interface Sci.*, 2014, **19**, 383–396.
- T. Abitbol, A. Rivkin, Y. Cao, Y. Nevo, E. Abraham, T. Ben-Shalom, S. Lapidot and O. Shoseyov, *Curr. Opin. Biotechnol.*, 2016, **39**, 76–88.
- Internet, Nanocellulose State of the Industry, <https://goo.gl/Tzz2WV> (Accessed June 2017).
- RISE, *Roadmap 2015 to 2025 Materials from nanocellulose*, 2015.
- S. Rebouillat and F. Pla, *J. Biomater. Nanobiotechnol.*, 2013, **4**, 165–188.
- I. Graveson and R. English, Low energy method for the preparation of non-derivatized nanocellulose, *US Pat. App.*, 14/413449, 2013.
- M. Mariño, L. Lopes da Silva, N. Durán and L. Tasic, *Molecules*, 2015, **20**, 5908–5923.



- 24 FAO and OECD, *OECD-FAO Agricultural Outlook 2015*, OECD Publishing, 2015.
- 25 C. Chen, A. R. Lo Piero and F. Gmitter, *Pigments in Fruits and Vegetables: Genomics and Dietetics*, 2015.
- 26 D. Mamma and P. Christakopoulos, *Waste Biomass Valorization*, 2014, **5**, 529–549.
- 27 L. A. Pfaltzgraff, M. De bruyn, E. C. Cooper, V. Budarin and J. H. Clark, *Green Chem.*, 2013, **15**, 307.
- 28 L. A. Pfaltzgraff, *The study & development of an integrated & additive-free waste orange peel biorefinery*, University of York, 2014.
- 29 A. M. Balu, V. Budarin, P. S. Shuttleworth, L. A. Pfaltzgraff, K. Waldron, R. Luque and J. H. Clark, *ChemSusChem*, 2012, **5**, 1694–1697.
- 30 A. S. Matharu, J. A. Houghton, C. Lucas-Torres and A. Moreno, *Green Chem.*, 2016, **337**, 695–699.
- 31 S. Tsubaki and J.-I. Azum, in *Advances in Induction and Microwave Heating of Mineral and Organic Materials*, InTech, 2011, (Ed.), ISBN: 978-953-307-522-8, InTech.
- 32 E. Destandau, T. Michel and C. Elfakir, in *Natural Product Extraction: Principles and Applications*, 2013, pp. 113–156.
- 33 V. L. Budarin, J. H. Clark, B. A. Lanigan, P. Shuttleworth and D. J. Macquarrie, *Bioresour. Technol.*, 2010, **101**, 3776–3779.
- 34 N. Flórez, E. Conde and H. Domínguez, *J. Chem. Technol. Biotechnol.*, 2015, **90**, 590–607.
- 35 S. Fan, P. Zhang, F. Li, S. Jin, S. Wang and S. Zhou, *Curr. Org. Chem.*, 2016, **20**, 2799–2809.
- 36 A. T. Quitain, T. Kai, M. Sasaki and M. Goto, *Ind. Eng. Chem. Res.*, 2013, **52**, 7940–7946.
- 37 F. S. Panthapulakkal, *Microwave Assisted Extraction of Xylan*, University of Toronto, 2014.
- 38 D. Brindha, S. Vinodhini, K. Alarmelumangai and N. S. Malathy, *Indian J. Fundam. Appl. Life Sci.*, 2012, **2**, 217–221.
- 39 N. F. Mat Zain, *J. Nutr. Food Sci.*, 2014, **5**, 10–13.
- 40 P. J. Van Soest, in *Nutritional Ecology of the Ruminant*, Cornell University Press, 2nd edn, 1994, pp. 140–155.
- 41 J. Fan, M. De bruyn, V. L. Budarin, M. J. Gronnow, P. S. Shuttleworth, S. Breeden, D. J. Macquarrie and J. H. Clark, *J. Am. Chem. Soc.*, 2013, **135**, 11728–11731.
- 42 P. Singh and A. Pandey, *Biotechnology for Agro-Industrial Residues Utilisation*, 2009.
- 43 M. R. K. Sofla, R. J. Brown, T. Tsuzuki and T. J. Rainey, *Adv. Nat. Sci. Nanosci. Nanotechnol.*, 2016, **7**, 35004.
- 44 H. Zhu, Z. Fang, C. Preston, Y. Li and L. Hu, *Energy Environ. Sci.*, 2014, **7**, 269–287.
- 45 G. Cheng, X. Zhang, B. Simmons and S. Singh, *Energy Environ. Sci.*, 2015, **8**, 436–455.
- 46 S. P. S. Chundawat, B. S. Donohoe, L. da Costa Sousa, T. Elder, U. P. Agarwal, F. Lu, J. Ralph, M. E. Himmel, V. Balan and B. E. Dale, *Energy Environ. Sci.*, 2011, **4**, 973.
- 47 Y. Pu, B. Hallac and A. J. Ragauskas, in *Aqueous Pretreatment of Plant Biomass for Biological and Chemical Conversion to Fuels and Chemicals*, John Wiley & Sons, Ltd, Chichester, UK, 2013, pp. 369–390.
- 48 H. N. Cheng and T. G. Neiss, *Polym. Rev.*, 2012, **52**, 81–114.
- 49 M. J. Pena, A. G. Darvill, S. Eberhard, W. S. York and M. A. O'Neill, *Glycobiology*, 2008, **18**, 891–904.
- 50 A. Synytsya, J. Bopikova and J. Brus, *Czech J. Food Sci.*, 2003, **21**, 1–12.
- 51 H. Tang, P. S. Belton, A. Ng and P. Ryden, *J. Agric. Food Chem.*, 1999, **47**, 510–517.
- 52 H. Halonen, *Structural changes during cellulose composite processing*, Royal Institute of Technology, 2012.
- 53 M. Carrier, A. Loppinet-Serani, D. Denux, J.-M. Lasnier, F. Ham-Pichavant, F. Cansell and C. Aymonier, *Biomass Bioenergy*, 2011, **35**, 298–307.
- 54 K. Werner, L. Pommer and M. Broström, *J. Anal. Appl. Pyrolysis*, 2014, **110**, 130–137.
- 55 S. Sabiha-Hanim and A. Aziatul-Akma, in *Polymer Science: Research Advances, Practical Applications and Educational Aspects*, ed. A. Méndez-Vilas and A. Solano-Martín, Formatex Research Center, Spain, 2016, pp. 404–411.
- 56 Y.-M. Kim, H. W. Lee, S. Kim, C. Watanabe and Y.-K. Park, *BioEnergy Res.*, 2015, **8**, 431–439.
- 57 M. Hajir, R. Graf and W. Tremel, *Chem. Commun.*, 2014, **50**, 6534.
- 58 J. A. Perez-Pimienta, M. G. Lopez-Ortega, J. A. Chavez-Carvayar, P. Varanasi, V. Stavila, G. Cheng, S. Singh and B. A. Simmons, *Biomass Bioenergy*, 2015, **75**, 180–188.
- 59 J. A. Perez-Pimienta, H. M. Poggi-Varaldo, T. Ponce-Noyola, A. C. Ramos-Valdivia, J. A. Chavez-Carvayar, V. Stavila and B. A. Simmons, *Biomass Bioenergy*, 2016, **91**, 48–55.
- 60 S. Xiao, R. Gao, Y. Lu, J. Li and Q. Sun, *Carbohydr. Polym.*, 2015, **119**, 202–209.
- 61 W. Wang and J.-H. Liu, *Gene*, 2015, **555**, 421–429.
- 62 A. M. Magomya, D. Kubmarawa, J. A. Ndahi and G. G. Yebpella, *Int. J. Sci. Technol. Res.*, 2014, **3**, 68–72.
- 63 N. Lin, J. Huang and A. Dufresne, *Nanoscale*, 2012, **4**, 3274.
- 64 A. Ramezani Kakroodi, S. Panthapulakkal, M. Sain and A. Asiri, *J. Appl. Polym. Sci.*, 2015, **132**, 1–7.
- 65 C. Sene, M. C. McCann, R. H. Wilson and R. Grinter, *Plant Physiol.*, 1994, **106**, 1623–1631.
- 66 R. Miranda, C. Sosa, D. Bustos, E. Carrillo and M. Rodriguez-Cantu, in *Lignocellulosic Precursors used in the Synthesis of Activated Carbon*, ed. V. Hernandez Montoya, InTech, 2012, p. 100.
- 67 Y. M. Kim, H. W. Lee, S. H. Lee, S. S. Kim, S. H. Park, J. K. Jeon, S. Kim and Y. K. Park, *Korean J. Chem. Eng.*, 2011, **28**, 2012–2016.
- 68 B. H. Davison, J. Parks, M. F. Davis and B. S. Donohoe, in *Aqueous Pretreatment of Plant Biomass for Biological and Chemical Conversion to Fuels and Chemicals*, John Wiley & Sons, Ltd, Chichester, UK, 2013, pp. 23–38.
- 69 S. Viamajala, B. S. Donohoe, S. R. Decker, T. B. Vinzant, M. J. Selig, M. E. Himmel and M. P. Tucker, in *Sustainable Biotechnology: Sources of Renewable Energy*, Springer, Netherlands, 2010, pp. 1–18.
- 70 S. S. Cho and M. L. Dreher, *Handbook of dietary fiber*, 2001, vol. 113.

